Journal of the Korean Crystal Growth and Crystal Technology
Vol. 30, No. 3 (2020) 117-122
https://doi.org/10.6111/JKCGCT.2020.30.3.117

p-ISSN 1225-1429
e-ISSN 2234-5078

Double-diffusive convection affected by conductive and insulating side walls during physical vapor transport of Hg_2Br_2

Geug Tae Kim† and Moo Hyun Kwon*

Department of Chemical Engineering, Hannam University, Daejeon 34054, Korea
***Department of Energy and Electrical Engineering, Woosuk University, Jincheon 27841, Korea*

(Received May 25, 2020)
(Revised June 1, 2020)
(Accepted June 5, 2020)

Abstract In last few decades, although thermal and/or solutal buoyancy-driven recirculating flows in a closed ampoule have been intensively studies as a model problem, there exist interesting total molar flux of Hg_2Br_2 that have been unreported in the literature. It is concluded that the total molar flux of Hg_2Br_2(A) increases linearly and directly as the temperature difference regions in the range of $10^oC \le \Delta T \le 50^o$, $3.5 \times 10^3 \le Gr_t \le 4.08 \times 10^3$, $4.94 \times 10^4 \le Gr_s \le 6.87 \times 10^4$. For the range of 10 Torr $\le P_B \le$ 150 Torr, the total molar flux of Hg_2Br_2(A) decays second order exponentially as the partial pressure of component B (argon as an impurity), P_B increases. From the view point of energy transport, the fewer the partial pressure of component B (argon), P_B is, the more the energy transport is achieved.

Key words Double diffusion, Physical vapor transport, Hg_2Br_2

1. Introduction

During the past few decades one area of interest in double diffusion has been the study of the physical vapor transport (PVT) processes in a sealed chamber. In recent years, the problems of Cattaneo-Christov double diffusion have been studied for Williamson nanomaterials slip flow subject to porous medium [1], and bi-directional stretched nanofluid flow with Cattaneo-Christov double diffusion [2]. Muhammad et al. [3] addressed Darcy-Forchheimer flow over an exponentially stretching curved surface with Cattaneo-Christov double diffusion. Asha and Sunitha [4] reported thermal radiation and hall effects on peristaltic blood flow with double diffusion in the presence of nanoparticles.

Mercurous halide materials are well known as the most promising materials in applications for acousto-optic materials and signal processing optics, for example, Bragg cells. Singh and his group investigated systematically the growth and characterization and development of large single crystals of Hg_2Br_2 [5-11]. Many reports of Hg_2Br_2 could be found in references [12-16]. Kim and his coworkers [17-19] have performed two-dimensional numerical studies of double diffusion convection in the vapor phase during physical vapor crystal growth. Duval [20] published that four flow structure regions appear during the physical vapor transport of mercurous chloride crystal growth.

Our numerical simulations are motivated by the desire to study the influences of hybrid thermal boundary conditions on the convective flow because the final quality of crystal is affected by convection fields. In this paper, the effects of the temperature differences between the source and crystal, the Peclet number, Pe, and the partial pressure of component B (argon as inert gas), P_B on the total molar flux of Hg_2Br_2 and the maximum magnitudes of velocity vector, $|U|_{max}$ in the dimensional unit (cm/sec) shall be addressed.

2. Numerical Simulations

Consider steady state thermal and solutal buoyancy driven recirculating flows of Hg_2Br_2(A)-argon (B) with thermo-physical properties listed in Table 1, in PVT crystal growth enclosure for hybrid thermal boundary conditions with linear temperature profiles, i.e., conductive walls, and insulating walls, shown in Fig. 1, accompanied by a 42×22 ($x \times y$) grid system. The detailed assumptions and nomenclature can be found in reference [17]. Also, the dimensionless parameters of Prandtl, Lewis, Peclet, Grashof, concentration, aspect ratio are described in reference [20].

In non-dimensional form, continuity, Navier-Stokes momenta, energy transport, and mass transport are gov-

†Corresponding author
E-mail: geugtaekim@gmail.com

Table 1
Thermo-physical properties of Hg_2Br_2(A)-argon (B) (M_A = 560.988, M_B = 39.944) at $\Delta T = 50^oC$, P_B = 10 Torr

Kinematic viscosity	0.44 cm^2/sec
Thermal diffusivity	0.45 cm^2/sec^2
Binary diffusivity	1.28 cm^2/sec^2
Coefficient of thermal volume expansion	0.0017 $(1/^oC)$
Density of mixture	0.000599 g/cm^3
Prandtl number	0.97
Lewis number	0.35
Peclet number	3.65
Concentration number	1.02
Thermal Grashof number	3.5×10^3
Solutal Grashof number	4.94×10^4

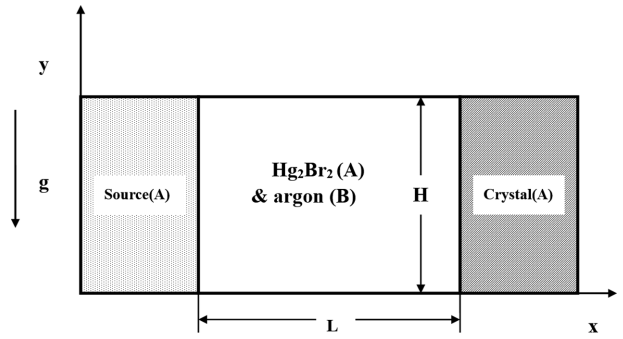

Fig. 1. System schematic and coordinates for numerical simulation of PVT crystal growth reactor of Hg_2Br_2(A)-argon (B).

erned by:

$$\nabla^* \bullet V = 0, \tag{1}$$

$$\vec{V} \bullet \nabla^* \vec{V} = -\nabla^* p^* + Pr\nabla^{*2}\vec{V} - \frac{Gr \cdot Pr^2}{Ar^3} \cdot \frac{(1-\rho^*)}{\beta \Delta T}, \tag{2}$$

$$\vec{V} \bullet \nabla^* T^* = \nabla^{*2} T^*, \tag{3}$$

$$\vec{V} \bullet \nabla^* \omega_A^* = \frac{1}{Le}\nabla^{*2}\omega_A^*. \tag{4}$$

The boundary conditions corresponding to the above equations (1) to (4) are given as follows:

On the walls

$(0 < x^* < 1, y^* = 0$ and $1)$:

$$u(x^*, 0) = u(x^*, 1) = v(x^*, 0) = v(x^*, 1) = 0 \tag{5}$$

$$\frac{\partial \omega_A^*(x^*, 0)}{\partial y^*} = \frac{\partial \omega_A^*(x^*, 1)}{\partial y^*} = 0,$$

$$T^*(x^*, 0) = -\frac{1}{Ar} \cdot x^* + 1$$

$(1 < x^* < 3, y^* = 0$ and $1)$:

$$u(x^*, 0) = u(x^*, 1) = v(x^*, 0) = v(x^*, 1) = 0 \tag{6}$$

$$\frac{\partial \omega_A^*(x^*, 0)}{\partial y^*} = \frac{\partial \omega_A^*(x^*, 1)}{\partial y^*} = 0,$$

$$\frac{\partial T^*(x^*, 0)}{\partial y^*} = \frac{\partial T^*(x^*, 1)}{\partial y^*} = 0$$

$(3 < x^* < 4, y^* = 0$ and $1)$:

$$u(x^*, 0) = u(x^*, 1) = v(x^*, 0) = v(x^*, 1) = 0 \tag{7}$$

$$\frac{\partial \omega_A^*(x^*, 0)}{\partial y^*} = \frac{\partial \omega_A^*(x^*, 1)}{\partial y^*} = 0,$$

$$T^*(x^*, 0) = -\frac{1}{Ar} \cdot x^* + 1$$

On the source $(x^* = 0, 0 < y^* < 1)$:

$$u(0, y^*) = -\frac{1}{Le(Cv-1)} \frac{\partial \omega_A^*(0, y^*)}{\partial x^*}, \tag{8}$$

$$v(0, y^*) = 0,$$
$$T^*(0, y^*) = 1,$$
$$\omega_A^*(0, y^*) = 1.$$

On the crystal $(x^* = L/H, 0 < y^* < 1)$:

$$u(L/H, y^*) = -\frac{1}{LeCv} \frac{\partial \omega_A^*(L/H, y^*)}{\partial x^*}, \tag{9}$$

$$v(L/H, y^*) = 0,$$
$$T^*(L/H, y^*) = 0,$$
$$\omega_A^*(L/H, y^*) = 0.$$

The code verification of one's results can be found in reference [17], for the Semi-Implicit Method Pressure-Linked Equations Revised (SIMPLER) [21].

3. Results and Discussion

When $M_A \neq M_B$, the two molecular weights of Hg_2Br_2 and argon are different, i.e., M_A = 560.988 g/gmol, M_B = 39.944 g/gmol, solutally buoyancy driven convection is much important compared with thermally buoyancy driven convection, but solutal and/or thermal convection are coupled and the effects of thermal buoyancy convection cannot be neglected during the physical vapor transport of Hg_2Br_2 in the vapor phase. Therefore, our interest is restricted on our studies to investigate the relations of the driving force, the temperature difference, ΔT, the maximum magnitudes of velocity vector, $|U|_{max}$ and the Peclet number for the transport of crystal species.

As shown in Fig. 2, it is clear that the total molar flux of Hg_2Br_2(A) increases linearly and directly as the temperature difference in the range of $10^oC \leq \Delta T \leq 50^oC$,

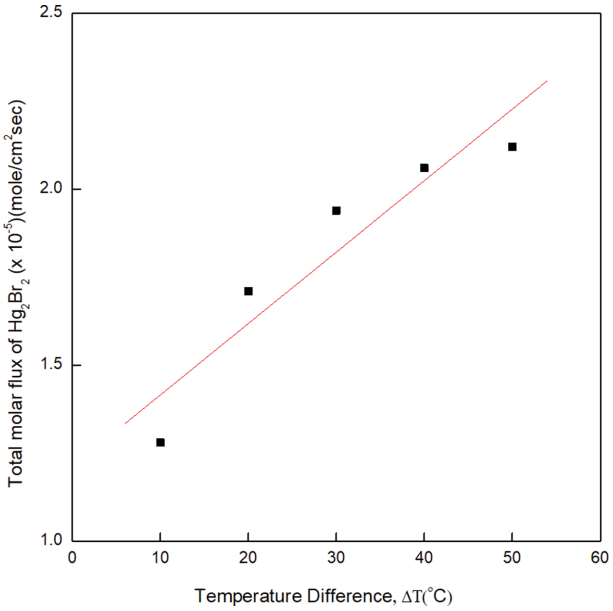

Fig. 2. The total molar flux of Hg_2Br_2(A) as a function of the temperature difference, ΔT (°C), based on aspect ratio = 4, T_s = 300°C, P_B = 10 Torr, $3.5 \times 10^3 \le Gr_t \le 4.08 \times 10^3$, $4.94 \times 10^4 \le Gr_s \le 6.87 \times 10^4$, on earth.

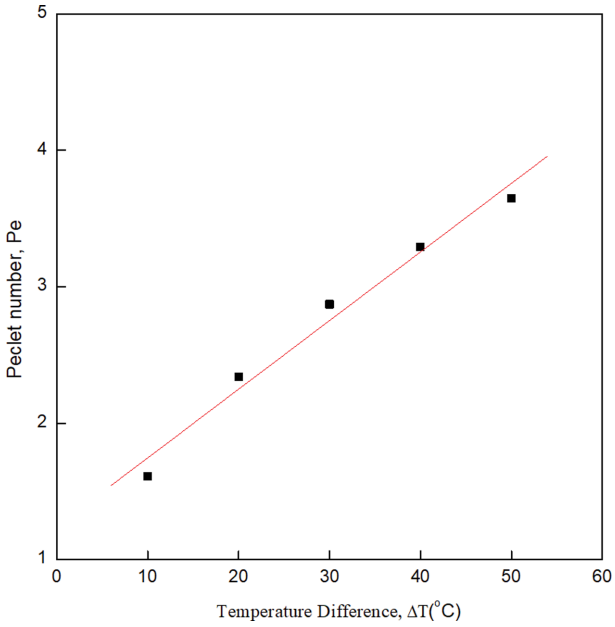

Fig. 3. The Peclet number, Pe as a function of the temperature difference, ΔT (°C), based on aspect ratio = 4, T_s = 300°C, P_B = 10 Torr, $3.5 \times 10^3 \le Gr_t \le 4.08 \times 10^3$, $4.94 \times 10^4 \le Gr_s \le 6.87 \times 10^4$, on earth.

$3.5 \times 10^3 \le Gr_t \le 4.08 \times 10^3$, $4.94 \times 10^4 \le Gr_s \le 6.87 \times 10^4$. For ΔT = 10°C, the corresponding thermal (Gr_t) and solutal (Gr_s) Grashof number is 4.08×10^3 and 6.87×10^4, respectively; for ΔT = 50°C, the corresponding thermal (Gr_t) and solutal (Gr_s) Grashof number is 3.5×10^3 and 4.94×10^4, respectively. With increasing the temperature difference, the corresponding thermal (Gr_t) and solutal (Gr_s) Grashof number reversely decrease, which reflected the variations in the density of the mixture of Hg_2Br_2 and argon. In other words, for ΔT = 10°C, the kinematic viscosity is 0.18 cm^2/sec; for ΔT = 50°C, the kinematic viscosity is 0.44 cm^2/sec. The system considered in Fig. 1 is Ar (aspect ratio, transport length-to-width) = 4, T_s (source temperature) = 300°C, P_B (partial pressure of component B, argon) = 10 Torr, on earth. For ΔT = 10°C, the thermal diffusivity and binary mass diffusivity is 0.18, and 1.28 cm^2/sec; for ΔT = 50°C, the thermal diffusivity and binary mass diffusivity is 0.45, and 1.28 cm^2/sec. For the range of 10°C ≤ ΔT ≤ 30°C, the total molar flux of Hg_2Br_2(A) increases sharply with increasing the temperature difference, whereas for the range of 30°C ≤ ΔT ≤ 50°C, the total molar flux of Hg_2Br_2(A) increases relatively gradually. As mentioned before, this difference is likely be due to the variations in the density of the mixture of Hg_2Br_2 and argon.

Figure 3 illustrates the effects of Peclet number, Pe on as the temperature difference, ΔT in the range of 10°C ≤ ΔT ≤ 50°C, $3.5 \times 10^3 \le Gr_t \le 4.08 \times 10^3$, $4.94 \times 10^4 \le Gr_s \le 6.87 \times 10^4$. The Peclet number, Pe increases linearly and directly with the temperature differences. Figure 4 shows the relation of the maximum magnitude of velocity vector, $|U|_{max}$ and Peclet number, Pe for 10°C ≤ ΔT ≤ 50°C, aspect ratio = 4, T_s = 300°C, P_B = 10 Torr, on earth. This relation illustrates that the $|U|_{max}$ increases linearly with the Peclet number, Pe. Note that the Peclet number is

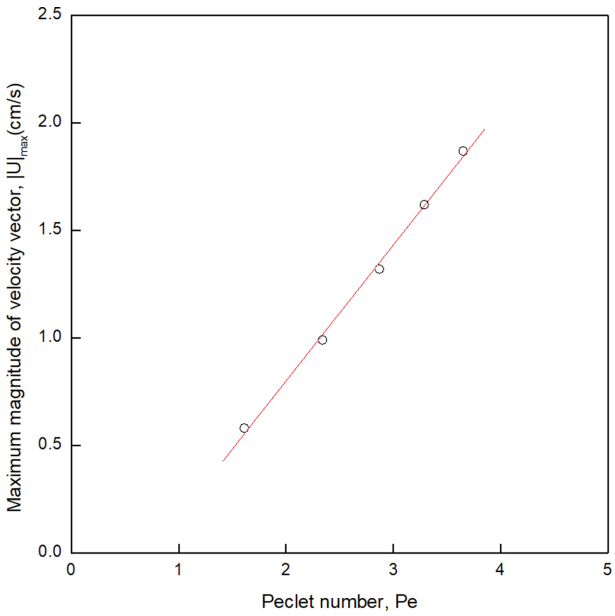

Fig. 4. The $|U|_{max}$ as a function of the dimensionless Peclet number, Pe, based on aspect ratio = 4, T_s = 300°C, P_B = 10 Torr, $3.5 \times 10^3 \le Gr_t \le 4.08 \times 10^3$, $4.94 \times 10^4 \le Gr_s \le 6.87 \times 10^4$, on earth.

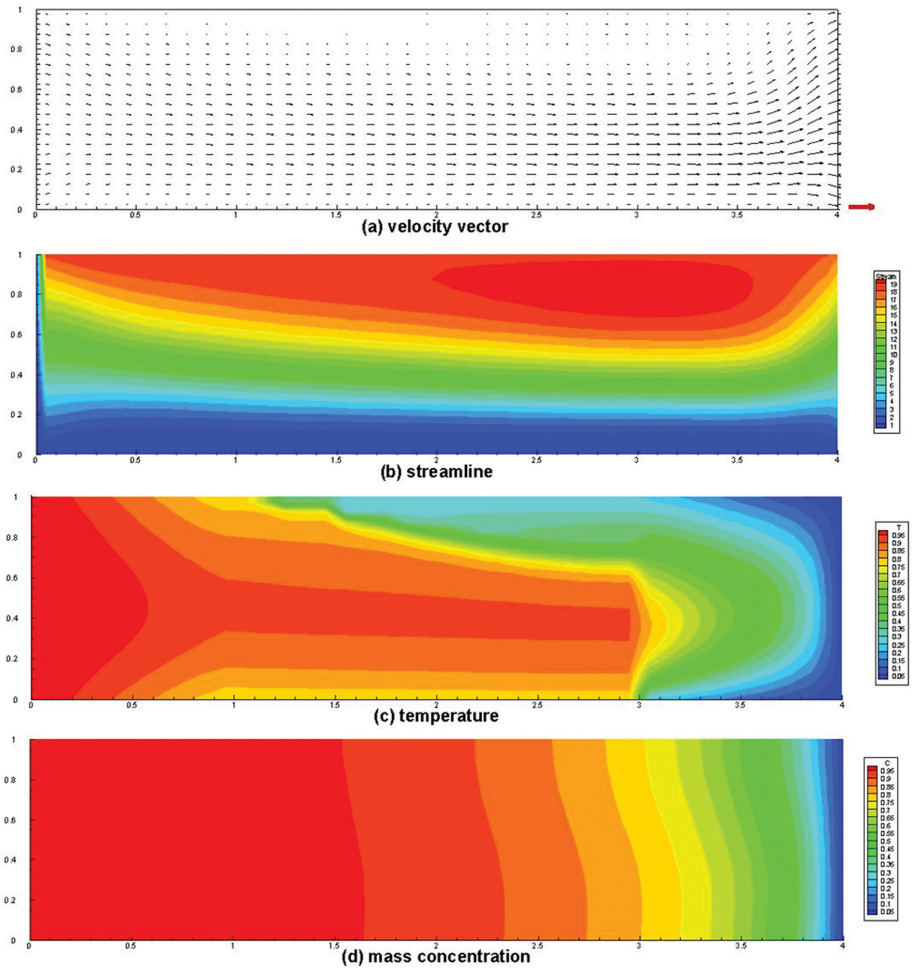

Fig. 5. (a) Velocity vector, (b) streamline, (c) temperature, (d) mass concentration profile, based on aspect ratio = 4, $\Delta T = 50^{o}C$ ($300^{o}C \rightarrow 250^{o}C$), $P_B = 10$ Torr, Peclet number = 3.65, thermal Grashof number $(Gr_t) = 3.5 \times 10^3$, solutal Grashof number $(Gr_s) = 4.94 \times 10^4$, Prandtl number = 0.97, Lewis number = 0.35, concentration parameter = 1.02, total pressure = 108 Torr, $|U|_{max} = 1.87$ cm/sec, on earth.

intimately related to the advections across the interfaces at the source and the crystal regions.

Figure 5 shows the profiles of velocity vector, streamline, temperature, mass concentration, based on aspect ratio = 4, $\Delta T = 50^{o}C$ ($300^{o}C \rightarrow 250^{o}C$), $P_B = 10$ Torr, $|U|_{max} = 1.87$ cm/sec, on earth. As plotted in Fig. 5, there exists small one convective cell in the vapor phase, and the flow structure is asymmetrical against at $y^* = 0.5$ and three-dimensional flow structure. For the flow regions along the transport length at the bottom region, i.e., $0 \le y^* \le 0.5$, the one-dimensional Stefan flows appear. Temperature profile shown in Fig. 5(c) is related to the hybrid thermal boundary conditions; for $0 \le x^* \le 1$, conductive walls and for $1 \le x^* \le 3$, insulating walls, for $3 \le x^* \le 4$, conductive walls. Close spacings of mass concentration shown in Fig. 5(d) exhibits the mechanism of the diffusion-limited mass transfer.

Figure 6 shows the effects of the partial pressure of component B (argon), P_B, on the total molar flux of Hg_2Br_2(A), for 10 Torr $\le P_B \le$ 150 Torr, based on aspect ratio = 4, $\Delta T = 50^{o}C$, $T_s = 300^{o}C$, $P_B = 10$ Torr, $1.8 \times 10^3 \le Gr_t \le 2.9 \times 10^3$, $2.6 \times 10^4 \le Gr_s \le 4.9 \times 10^4$, on earth. For the range of 10 Torr $\le P_B \le$ 150 Torr, the total molar flux of Hg_2Br_2(A) decays second order exponentially with the partial pressure of component B (argon), P_B. Figure 7 shows the influences of the partial pressure of component B (argon), P_B, on the Peclet number, Pe, for 10 Torr $\le P_B \le$ 150 Torr, corresponding to Fig. 6.

Figure 8 shows the profiles of velocity vector, streamline, temperature, mass concentration, based on aspect ratio = 4, $\Delta T = 50^{o}C$ ($300^{o}C \rightarrow 250^{o}C$), $P_B = 60$ Torr, $|U|_{max} = 0.99$ cm/sec, on earth. As shown in Fig. 8, one convective roll is present in the vapor phase. In a comparison of Fig. 8(c) temperature with Fig. 5(c) temperature, from the view point of energy transport, the fewer the partial pressure of component B (argon), P_B is, the more

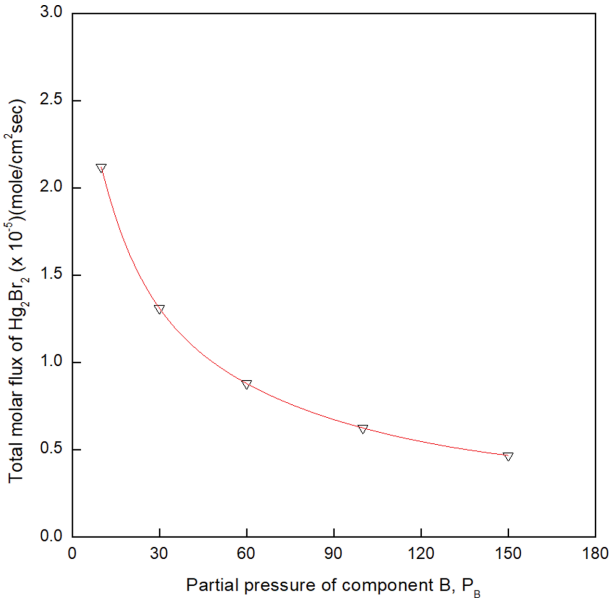

Fig. 6. The total molar flux of Hg_2Br_2(A) as the partial pressure of component B, P_B, based on aspect ratio = 4, $\Delta T = 50^oC$, $T_s = 300^oC$, $P_B = 10$ Torr, $1.8 \times 10^3 \le Gr_t \le 2.9 \times 10^3$, $2.6 \times 10^4 \le Gr_s \le 4.9 \times 10^4$, on earth.

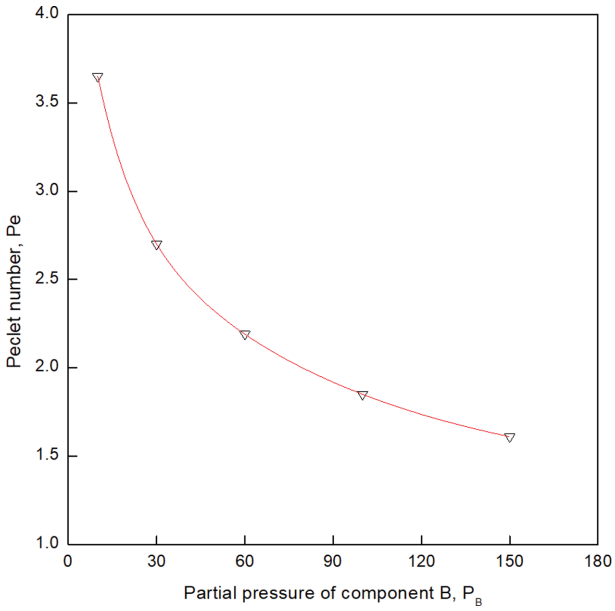

Fig. 7. The Peclet number, Pe as the partial pressure of component B, P_B, ΔT (^oC), based on aspect ratio = 4, $T_s = 300^oC$, $P_B = 10$ Torr, $3.5 \times 10^3 \le Gr_t \le 4.6 \times 10^3$, $4.9 \times 10^4 \le Gr_s \le 5.6 \times 10^4$, on earth.

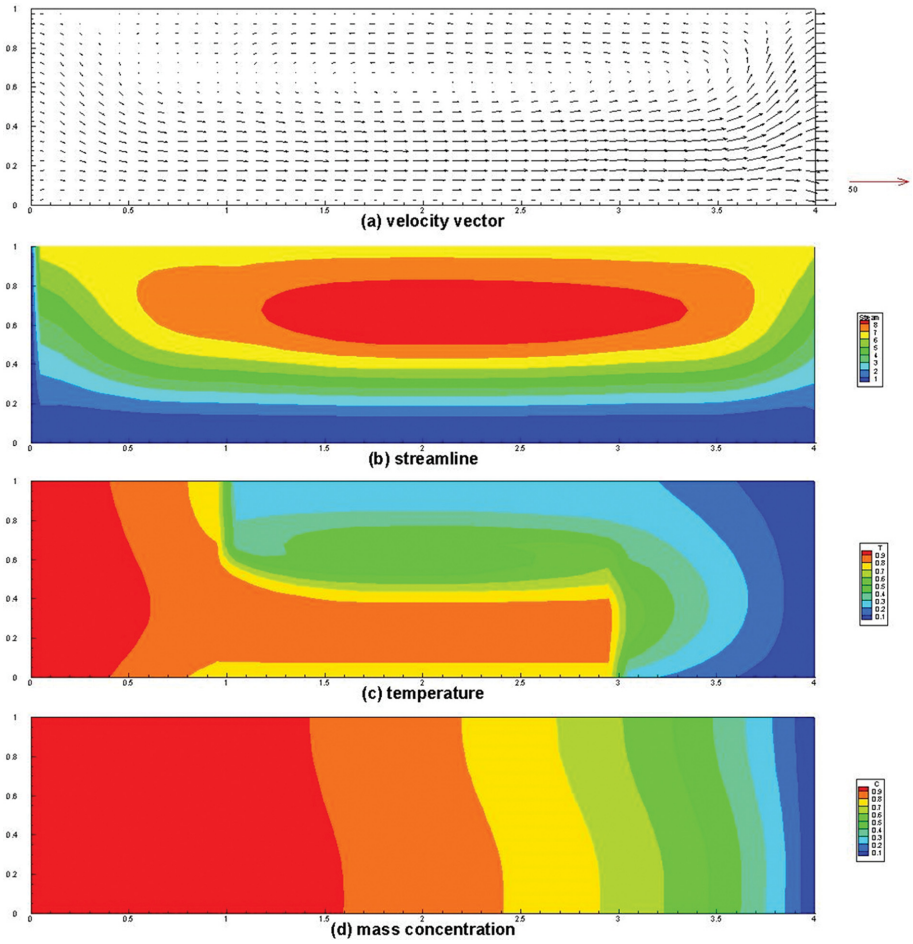

Fig. 8. (a) Velocity vector, (b) streamline, (c) temperature, (d) mass concentration profile, based on aspect ratio = 4, $\Delta T = 50^oC$ ($300^oC \rightarrow 250^oC$), $P_B = 60$ Torr, Peclet number = 2.19, thermal Grashof number (Gr_t) = 3.8×10^3, solutal Grashof number (Gr_s) = 5.07×10^4, Prandtl number = 0.92, Lewis number = 0.51, concentration parameter = 1.12, total pressure = 158 Torr, $|U|_{max} = 0.99$ cm/sec, on earth.

the energy transport is achieved.

4. Conclusions

It is concluded that the total molar flux of Hg_2Br_2(A) increases linearly and directly as the temperature difference, ΔT in the range of $10^oC \le \Delta T \le 50^oC$, $3.5 \times 10^3 \le Gr_t \le 4.08 \times 10^3$, $4.94 \times 10^4 \le Gr_s \le 6.87 \times 10^4$. For the range of 10 Torr $\le P_B \le$ 150 Torr, the total molar flux of Hg_2Br_2(A) decays second order exponentially with the partial pressure of component B (argon), P_B. From the view point of energy transport, the fewer the partial pressure of component B (argon), P_B is, the more the energy transport is achieved.

Acknowledgement

This work was financially supported by the LINC+ project Grant No. 2019BG042010106 (July 1, 2019 through December 31, 2019).

References

[1] M.I. Khana, F. Alzahrani, A. Hobiny and Z. Ali, "Modeling of Cattaneo-Christov double diffusions (CCDD) in Williamson nanomaterial slip flow subject to porous medium", J. Materials Res. Tech. (2020) in press.

[2] I. Ahmad, M. Faisal and T. Javed, "Bi-directional stretched nanofluid flow with Cattaneo-Christov double diffusion", Results Phys. 15 (2019) 102581.

[3] T. Muhammad, K. Rafique, M. Asma and M. Alghamdi, "Darcy-Forchheimer flow over an exponentially stretching curved surface with Cattaneo-Christov double diffusion", Physica A (2020) in press.

[4] S.K. Asha and G. Sunitha, "Thermal radiation and Hall effects on peristaltic blood flow with double diffusion in the presence of nanoparticles", Case Studies in Thermal Engineering 17 (2020) 100560.

[5] K.A. McCarthy, A.P. Goutzoulis, M. Gottlieb and N.B. Singh, "Optical rotatory power in crystals of the mercurous halides and tellurium dioxide", Opt. Commun. 64 (1987) 157.

[6] R. Mazelsky and D.K. Fox, "Development of large single crystals for electronic, electro-optic and acousto-optic devices", Prog. Crystal Growth and Charact. 15 (1987) 75.

[7] N.B. Singh, M. Gottlieb, A.P. Goutzoulis, R.H. Hopkins and R. Mazelsky, "Mercurous Bromide acousto-optic devices", J. Cryst. Growth 89 (1988) 527.

[8] N.B. Singh, M. Marshall, M. Gottlieb, G.B. Brandt, R.H. Hopkins, R. Mazelsky, W.M.B. Duval and M.E. Glicksman, "Purification and characterization of mercurous halides", J. Cryst. Growth 106 (1990) 61.

[9] N.B. Singh, M. Gottlieb and R. Mazelsky, "The optical quality of mercurous halides crystals", J. Cryst. Growth 128 (1993) 1053.

[10] N.B. Singh, M. Gottlieb, R.H. Hopkins, R. Mazelsky, W.M.B. Duval and M.E. Glicksman "Physical vapor transport growth of mercurous chloride crystals", Prog. Crystal Growth and Charact. 27 (1993) 201.

[11] N.B. Singh, M. Gottlieb, G.B. Branddt, A.M. Stewart, R.H. Hopkins, R. Mazelsky and M.E. Glicksman, "Growth and characterization of mercurous halide crystals: mercurous bromide system", J. Cryst. Growth 137 (1994) 155.

[12] A.A. Kaplyanskii, V.V. Kulakov, Yu.F. Markov and Ĉ. Barta, "The soft mode properties in Raman spectra of improper ferroelastics Hg_2Cl_2 and Hg_2Br_2", Solid State Commun. 21 (1977) 1023.

[13] M. Dalmon, S. Nakashima, S. Komatsubara and A. Mitsuishi, "Softening of acoustic and optical modes in ferroelstic phase in Hg_2Br_2", Solid State Commun. 28 (1978) 815.

[14] J.S. Kim, S.B. Trivedi, J. Soos, N. Gupta and W. Palosz, "Growth of Hg_2Cl_2 and Hg_2Br_2 single crystals by physical vapor transport", J. Cryst. Growth 310 (2008) 2457.

[15] T.H. Kim, H.T. Lee, Y.M. Kang, G.E. Jang, I.H. Kwon and B. Cho, "In-depth investigation of Hg_2Br_2 crystal growth and evolution", Materials 12 (2019) 4224.

[16] P.M. Amarasinghe, J.S. Kim, H. Chen, S. Trivedi, S.B. Qadri, J. Soos, M. Diestler, D. Zhang, N. Gupta and J.L. Jensen, "Growth of high quality mercurous halide sing crystals by physical vapor transport method for AOM and radiation detection applications", J. Cryst. Growth 450 (2016) 96.

[17] G.T. Kim and M. H. Kwon, "Effects of solutally dominant convection on physical vapor transport for a mixture of Hg_2Br_2 and Br_2 under microgravity environments", Korean Chem. Eng. Res. 52 (2014) 75.

[18] G.T. Kim and M.H. Kwon, "Numerical analysis of the influences of impurity on diffusive-convection flow fields by physical vapor transport under terrestrial and microgravity conditions: with application to mercurous chloride", Appl. Chem. Eng. 27 (2016) 335.

[19] S.H. Ha and G.T. Kim, "Preliminary studies on double-diffusive natural convection during physical vapor transport crystal growth of Hg_2Br_2 for the spaceflight experiments", Korean Chem. Eng. Res. 57 (2019) 289.

[20] W.M.B. Duval, "Transition to chaos in the physical transport process—I", the Proceeding of the ASME--WAM Winter Annual meeting, Fluid mechanics phenomena in microgravity, ASME-WAM, Nov. 28 -- Dec. 3, New Orleans, Louisiana (1993).

[21] S.V. Patankar, "Numerical Heat Transfer and Fluid Flow" (Hemisphere Publishing Corp. Washington D.C. 1980) p. 131.